Evaluation of charge storage ability of chrome doped Mn2O3 nanostructures derived by cathodic electrodeposition

Progress in Natural Science: Materials International 26 (2016) 523–527

HOSTED BY

ELSEVIER

Contents lists available at ScienceDirect

Progress in Natural Science: Materials International

journal homepage: www.elsevier.com/locate/pnsmi

Original Research

Evaluation of charge storage ability of chrome doped Mn_2O_3 nanostructures derived by cathodic electrodeposition☆

Hamideh Darjazi[c], Saied Saeed Hosseiny Davarani[a,*], Hamid Reza Moazami[b], Taher Yousefi[d], Farideh Tabatabaei[a]

[a] Faculty of Chemistry, Shahid Beheshti University, G. C., 1983963113, Evin, Tehran, Iran
[b] School of Physics and accelerators, NSTRI, P. O. Box 11365-8486, Tehran, Iran
[c] Department of Materials Enginnering, Naghshe Jahan Institute of Higher Education, Baharestan, Isfahan, Iran
[d] NFCRS, Nuclear Science and Technology Research Institute, P.O. Box 11365/8486, Tehran, Iran

ARTICLE INFO

Keywords:
Electro synthesis
Nanoparticles
Energy storage
Supercapacitor
Manganese oxide

ABSTRACT

A facile synthetic route has been proposed to prepare cauliflower-like nanostructures of Cr doped Mn_2O_3. The synthesis was carried out by constant current cathodic electrodeposition from Mn^{2+} nitrate solutions containing minor amounts of dichromate. It was found that the presence of Cr mediates the formation of cathodic MnO_2 which then reacts with the excess Mn^{2+} species to form Mn_2O_3 nanostructures. X-Ray Diffraction (XRD), Scanning Electron Microscopy (SEM) and Differential Thermal Analysis (DTA) were used to characterize the nanostructures. The storage ability of the obtained nanostructures was investigated by cyclic voltammetry (CV) in 0.5 M Na_2SO_4 solution. The results indicated that the Cr *doped manganese oxide* material shows better performance than the non-doped one, and the charge capacity (SC) of doped manganese oxide (218 F/g) was higher than pure manganese oxide (208 F/g).

1. Introduction

Recently, supercapacitors have attracted significant attention because of their bridging function between traditional dielectric capacitors and batteries/fuel cells. The capacitance of a typical supercapacitor is 20–200 times greater than that of a conventional capacitor of the same volume or mass [1]. On the other hand, supercapacitors offer higher power capability, reversibility and cycle life with respect to batteries/fuel cells. The capacitance and charge storage of a supercapacitor greatly depends on the electrode material used [1,2]. Transition metal oxides are considered as the best electrode materials due to their high specific capacitance and low resistance which together provide high power output required for commercial applications [3]. Among various transition metal oxides systems, manganese oxides are the most economically reasonable and environmentally friendly ones. Manganese dioxide is the most studied case. Other manganese oxides such as Mn_3O_4 and Mn_2O_3 are to be less favorable as the tetragonal distortion of the d^4 configuration in Mn (III) restricts the conductivity [4] but the oxidation state is not the only parameter that affects the charge storage ability. However, recent works have shown the enhanced storage ability of Mn_3O_4 and Mn_2O_3 as a result of morphological modification [5–10] or metal doping [11,12]. The classical method for the synthesis of Mn_2O_3 comprises thermal decomposition of manganese compounds at high temperatures [13–15]. Due to the diversity in oxidation state of manganese, careful control of the reaction temperature/atmosphere is needed to avoid formation of other oxides such as MnO, Mn_3O_4 and MnO_2 [16,17].

In this investigation, the direct synthesis of Mn_2O_3 nanostructures (without heat treatment) by mediating of dichromate ions as catalyst would be reported. The product is characterized by Scanning Electron Microscopy (SEM), differential thermal analysis (DTA) and X-ray diffraction. The electrochemical properties of the sample have been studied by cyclic voltametery. The results showed that doping of manganese dioxide with 10 wt% Cr significantly improved charge storage performance of the electrode.

2. Experimental

2.1. Materials

Analytical grade $Mn(NO_3)_2{\cdot}4H_2O$ and $K_2Cr_2O_7$ were purchased from Merck (Darmstadt, Germany). Deionized water was obtained through a Millipore water purification system (Milford, MA, USA). The graphite anodes were purchased from local suppliers.

Peer review under responsibility of Chinese Materials Research Society.
* Corresponding author.

http://dx.doi.org/10.1016/j.pnsc.2016.09.006
Received 25 February 2016; Received in revised form 27 August 2016; Accepted 27 September 2016
Available online 09 December 2016
1002-0071/

2.2. Preparation of Mn_2O_3

Thin films of manganese oxide and manganese oxide doped with chromium were prepared by the cathodic electrodeposition method from a solution of Mn^{2+} at a concentration of 10^{-2} M by dissolving appropriate amounts of $Mn(NO_3)_2{\cdot}4H_2O$ in deionized water. Different amounts of Cr^{6+}(as $K_2Cr_2O_7$) were added to the solution until reaching Cr/Mn ratio of 0, 2.5, 5,7.5%, and 10%. The electrochemical cell included the cathodic substrate centered between the two co-planar graphite counter electrodes. The cathodic deposits were obtained on a steel electrode (316 L, 100 mm×50 mm×0.5 mm) by the galvanostatic mode deposition at the current density of 0.25 mA cm^{-2}. The deposition time was 25 min. The obtained deposits were washed with deionized water, acetone and dried in air. The obtained samples were dried at 120 °C for 2hr.

2.3. Characterization

X-ray diffraction patterns of the samples were recorded by means of a STOE XD-3A X-ray diffractometer (CuKα radiation, λ=1.5406 nm). Scanning electron micrographs were taken using a TESCAN MIRA3 field-emission scanning electron microscope (FESEM) equipped with energy dispersive x-ray (EDX). The Infrared spectra of the samples were recorded by means of a BOMEM MB-series FTIR spectrometer within the wave number range of 250–4000 cm^{-1} after pelleting with KBr. The specific surface area was determined with a Quanta-chrome NOVA-2200e system, through measuring N_2 adsorption-desorption isotherms at 77 K.

2.4. Electrochemical measurements

Electrochemical studies were performed using an Autolab 302 N potentiostat. Cyclic voltammetric measurements were carried out by means of a standard three electrode cell configuration with a platinum wire, an Ag/AgCl and a glassy carbon (with 0.071 cm^2 area) as counter, reference, and working electrodes, respectively. 85 wt% of the obtained sample was mixed with 10 wt% of acetylene black as a conductivity enhancer and 5 wt% of polyvinylidenefloride as the binder. Few drops of N-methyl-2-pyrrolidone were added to obtain a homogenous slurry. The obtained slurry was dried at 80 °C for 12 h and then pressed on the surface of the glassy carbon electrode. In order to investigate the storage ability of the samples, cyclic voltammetry was performed in a Na_2SO_4 (0.5 M) aqueous solution within a potential range of −0.1 to +0.9 v vs. Ag/AgCl at different scan rates ranging from 1 to 100 mVS^{-1}. The Specific Capacitance (SC) was then calculated by integration of the current over the whole range of the applied cyclic potential according to Eq. (1):

$$SC=\frac{1}{mv(V_a-V_c)}\int_{V_a}^{V_c} I(V)dV \quad (1)$$

where, I is the measured current (A), (V_a–V_c) is the sweep potential range (V), m is the mass of electrochemically active material (g) and υ is the sweep rate (V S^{-1}).

3. Results and discussion

3.1. XRD study

Fig. 1 shows the XRD patterns of the samples as prepared from the solutions containing different amounts of Cr^{6+}. The addition of Cr at a Cr/Mn ratio of 2.5% resulted in the emergence of different characteristic peak as demonstrated in Fig. 1(a). The new peaks at 2θ=23.1, 32.9,38.2, 45.1, 49.3, 55.1 and 65.7° can be attributed to [211], [222], [400], [332], [431], [440] and [622] planes of Mn_2O_3, respectively. By increasing the amount of the added Cr, the intensity of the characteristic peaks decreased until fading at a Cr/Mn ratio of 10% (Fig. 1(d)).

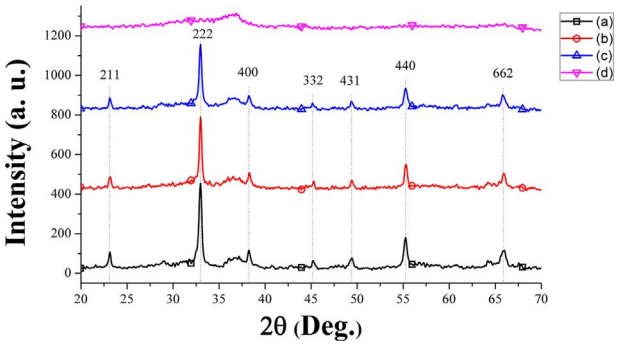

Fig. 1. X-Ray diffraction patterns of the samples synthesized frommanganese (II) nitrate solutions containing 2.5% (a), 5% (b), 7.5% (c) and 10% Cr^{6+}(d).

3.2. Electrodeposition mechanism

We have recently proposed a novel method for the electrosynthesis of hausmannite nanoparticles [11]. The method is based on the transition metal mediated formation of Mn^{3+}. Theoretically, any transition metal with two different oxidation states can act as a mediator in oxidation of Mn^{3+}. In the case of Cr, the reaction is:

$$Cr^{6+}+3Mn^{2+}\rightarrow Cr^{3+}+3Mn^{3+} \quad (2)$$

Reaction (2) seems to be less probable as Mn^{3+} is a strong oxidizer that can easily revert the reaction by the conversion of Cr^{3+} to Cr^{6+} [18]. In fact, the reaction takes place just because it is followed by exothermic disproportionation of Mn^{3+}:

$$2Mn^{3+}+2H_2O\rightarrow Mn^{2+}+MnO_2+4H^+ \quad \Delta G=-53 kJ\ mol^{-1} \quad (3)$$

According to Eq. (3), the disproportionation of $Mn^{3+}$is facilitated by low proton concentrations. The local proton concentration at the cathode surface is lower than the bulk of the solution due to cathodic generation of OH^-:

$$H_2O+2e^-\rightarrow H_2+2OH^- \quad E^0=-1{\cdot}05 \text{ V vs. Ag/AgCl} \quad (4)$$

$$O_2+2H_2O+4e^-\rightarrow 4OH^- \quad E^0=+0{\cdot}18 \text{ V vs. Ag/AgCl} \quad (5)$$

$$NO_3^-+H_2O+2e^-\rightarrow NO_2^-+2OH^- \quad E^0=-0{\cdot}21 \text{ V vs. Ag/AgCl} \quad (6)$$

This may tend to form manganese dioxide on the cathode surface which can be converted to Mn_2O_3 by further reduction [19] or by a chemical reaction with the excess Mn^{2+}[20]:

$$2MnO_2+H_2O+2e^-\rightarrow Mn_2O_3+2OH^- \quad E^0=+0{\cdot}15 \text{ V vs·Ag/AgCl} \quad (7)$$

$$MnO_2+Mn^{2+}+H_2O\rightarrow Mn_2O_3+2H^+ \quad (8)$$

3.3. Morphology

Fig. 2 shows the scanning electron micrographs of the samples electrodeposited from manganese nitrate solutions containing Cr^{6+} at Cr/Mn ratio of 0% (a), 2.5% (b), 5% (c), 7.5% (d) and 10% (e). In the absence of Cr, the electrodeposited layer was composed of densely packed nanoparticles (Fig. 2(a)). The addition of Cr resulted in a decreased in the surface density of the nanoparticles, forming porous layers as shown in (Fig. 2(b)). Additional amounts of Cr tend to form flower-like nanostructures as presented in Fig. 2(d) and (e). The morphological evolution by the addition of Cr can be described as follows:

There are three possible cathodic reactions during the generation of base. These include reduction of water, dissolved oxygen or nitrate ion

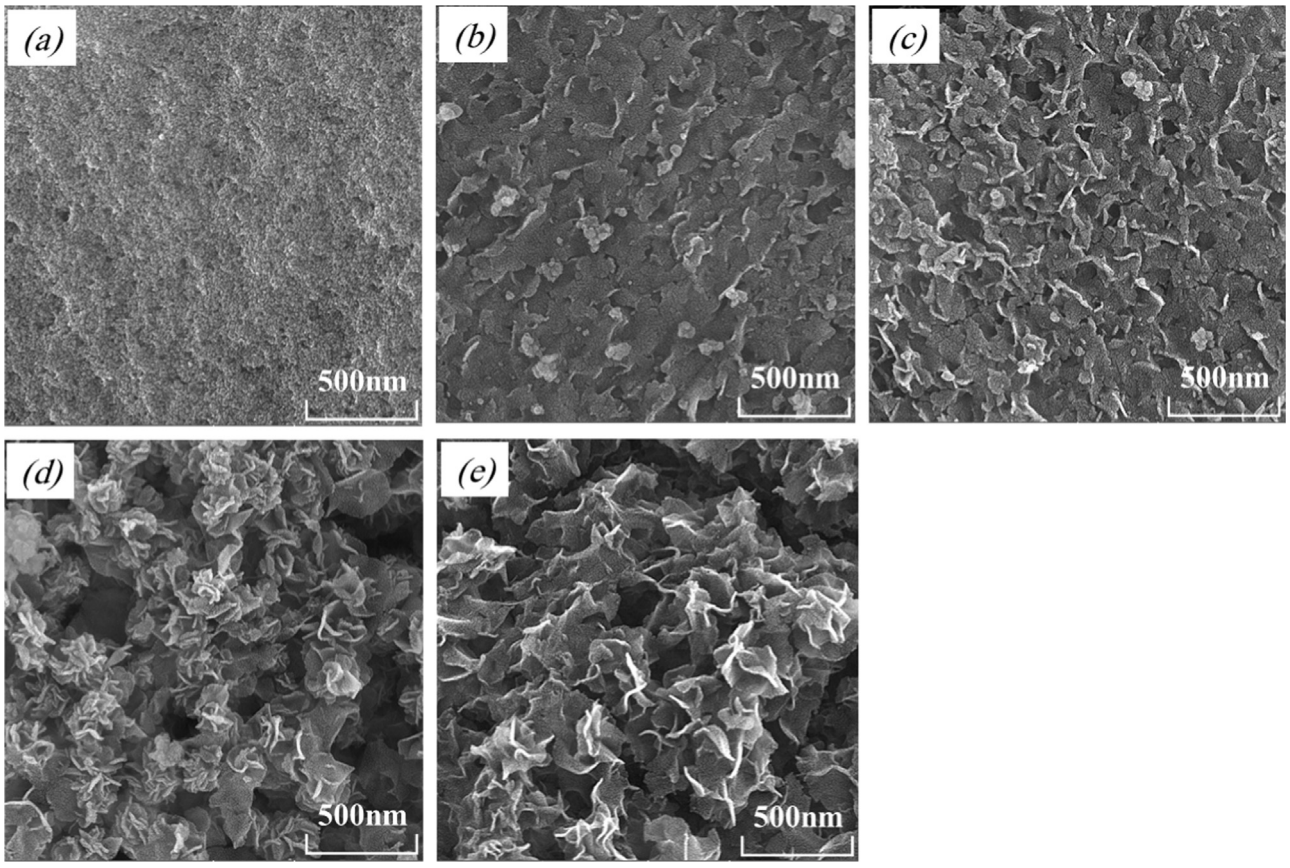

Fig. 2. SEM micrographs of the samples electrodeposited from 10^{-2}M manganese(II) nitrate containing Cr(VI) at Cr/Mn ratio of 0% (a), 2.5% (b), 5% (c), 7.5% (d) and 10% (e).

as illustrated by reactions (4), (5) and (6) respectively. Among them, the first reaction is accompanied by gaseous hydrogen evolution, whereas the remaining two reactions produce soluble products. Hydrogen evolution has a detrimental effect on the morphology of cathodically electrodeposited nanostructures. The bubble formation provides a dynamic template for the particles being deposited on the electrode surface [21]. As a consequence, nanoparticle formation is favorable at low hydrogen evolution rates but the nanorods or nanowire formation is favorable in high hydrogen formation rates. Based on the above point, any change in the kinetics of hydrogen evolution or the order of dominant reactions may lead to a change in morphology of the obtained structures.

Transition metal ions are known for their positive/negative effect on kinetics of hydrogen evolution reaction or water reduction on the electrode surface [22]. In the majority of cases, the transition metal ions decrease the rate of hydrogen evolution by either poisoning the electrode surface [23] or by catalyzing the competing reactions such as the reduction of nitrate [24]. On the contrary, some transition metals act as catalysts for hydrogen evolution [25]. Fig. 3 shows the cyclic voltammograms recorded in starting solutions at a scan rate of $20mVS^{-1}$. According to the obtained CVs, the reduction of water at -1.1V vs. Ag/AgCl is the dominant cathodic reaction in all solutions. Although the cathodic reaction is the same in all solutions, the rate of hydrogen evolution dramatically increases by increasing the amount of added Cr^{6+}.

As presented in Fig. 4. The higher rates of hydrogen evolution tend to form hierarchical nanostructures rather than densely packed nanoparticles observed at low evolution rate.

3.4. Thermal analysis and BET

In order to investigate the thermal behavior of the obtained

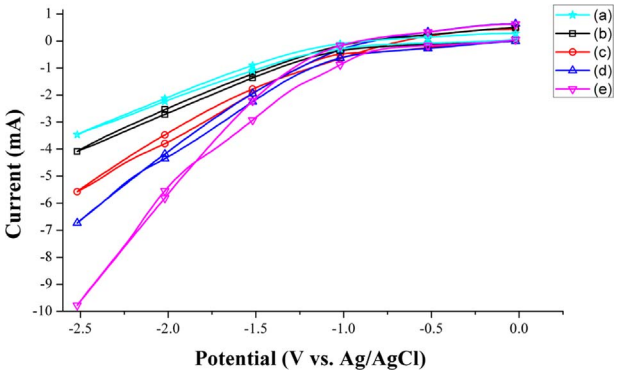

Fig. 3. Cyclic voltammograms obtained from manganese (II) solutions containing Cr (VI) at a Cr/Mn ratio of 0% (a), 2.5% (b), 5% (c), 7.5% (d) and 10% (e).

precursors, differential thermal analysis (DTA) was carried out at a heating rate of $10Cmin^{-1}$ at the temperatures ranging from 25 to 300 °C. Fig. 6 shows the results recorded for the precursors as electrodeposited from manganese nitrate solution containing 2.5% (a), 5% (b), 7.5% (c) and 10% Cr. For all samples, the broad endothermic peaks, extended from the ambient temperature to approximately 100 °C, represent the loss of the physically/chemically adsorbed water. The intensity of the broad peak increases by increasing the Cr/Mn ratio indicating stronger water adsorption due to the improved porosity of the structure. In every case, the broad peak is followed by the distinct endothermic peaks around 200 °C whose magnitude is inversely proportional to the dopant content these peaks can be attributed to the phase transformation of manganese oxide and the production of Mn_3O_4. The observed thermal behavior is in accordance with the previous reports on DTA of metal doped Mn_2O_3 [26]. The nanostructure nature of obtained sample is further validated

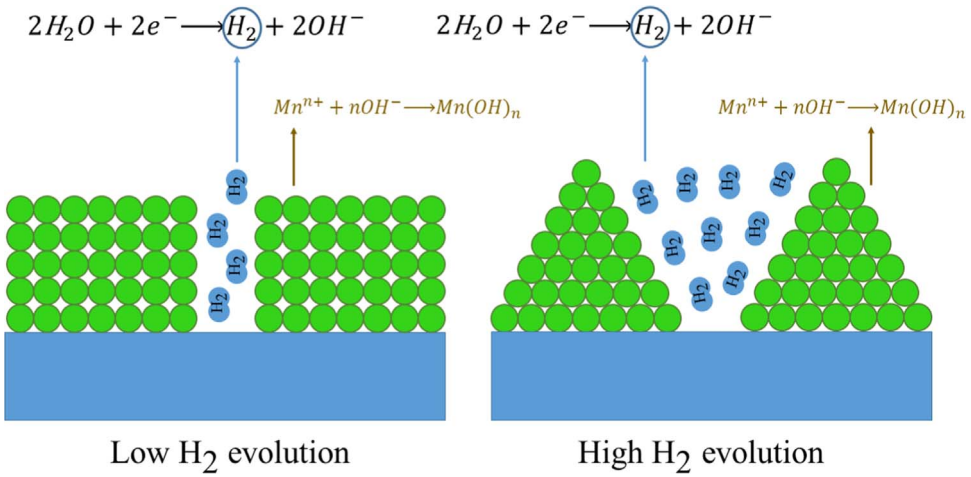

Fig. 4. the effect of hydrogen evolution kinetics on the morphology of sample.

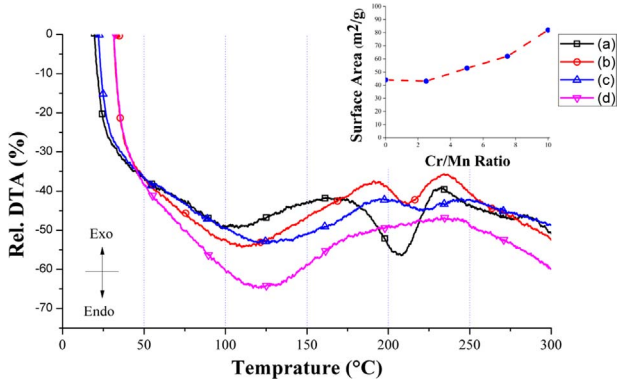

Fig. 5. differential thermal analysis of the samples electrodeposited from manganese nitrate solutions containing Cr^{6+} at a Cr/Mn ratio of 2.5% (a), 5% (b), 7.5% (c) and 10% (d). Inset: surface area of samples with different Cr value.

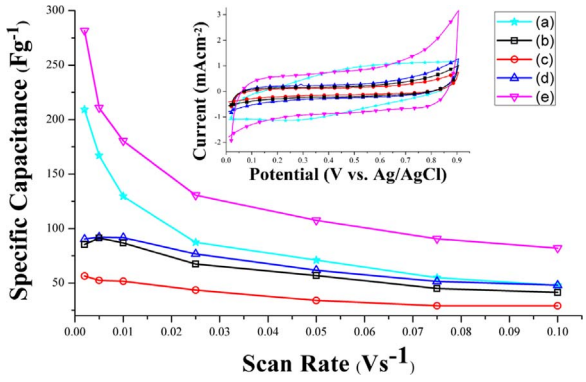

Fig. 6. the SC values as a function of scan rate for the samples electrodeposited from manganese nitrate solutions containing Cr^{6+} at Cr/Mn ratio of 0% (a), 2.5% (b), 5% (c), 7.5% (d) and 10% (e).

by N_2 adsorption/desorption isotherms. The BET surface area and porosity were investigated by nitrogen adsorption/desorption isotherms at 77 K (as shown in Fig. 5). Before adsorption measurements the sample was activated by heating to 423 K with heating rate of 0.5 K min^{-1} and keeping at this temperature under the turbomolecular pump vacuum. The specific surface area of samples (estimated from the Brunauer-Emmett-Teller (BET) method) were: sample1(Cr/Mn ratio of 0%)=44 m^2 g^{-1}; sample2(Cr/Mn ratio of 2.5%)=43 m^2 g^{-1}; sample3 (Cr/Mn ratio of 5%)=53 m^2 g^{-1}; sample 4(Cr/Mn ratio of 7.5%)=62 m^2 g^{-1} and sample5 (Cr/Mn ratio of 10%) =82 m^2 g^{-1} the results are in good agreement with morphology and capacity results(Fig. 5 inset).

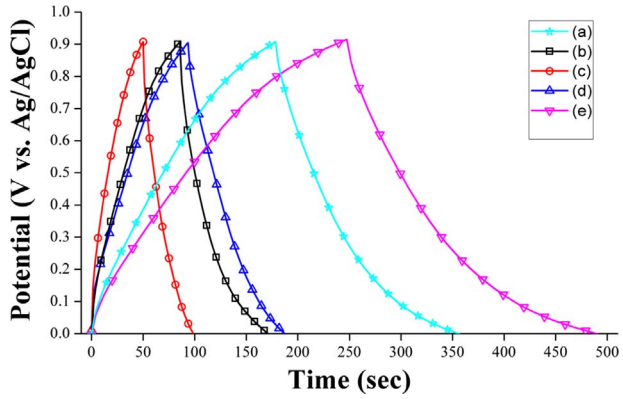

Fig. 7. the charge/discharge curves in the potential range of 0–0.9 V and current density of 1 A g^{-1} recorded for the samples electrodeposited from manganese nitrate solutions containing Cr6+ at Cr/Mn ratio of 0% (a), 2.5% (b), 5% (c), 7.5% (d) and 10% (e).

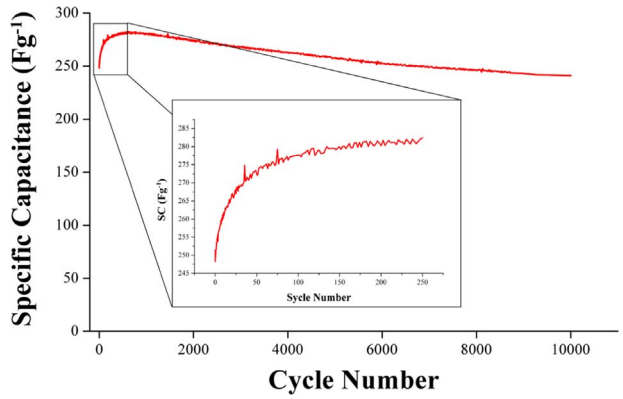

Fig. 8. cycling stability electrode during 10,000 cycles (inset: increase capacitance in first 250 cycles).

3.5. Capacitive behavior

The mechanism of energy storage in manganese oxides can be expressed as [19]:

$$MnO_\alpha(OC)_\beta + \delta C^+ + \delta e^- \leftrightarrow MnO_{\alpha-\beta}(OC)_{\beta+\delta} \quad (9)$$

Where, C^+ denotes proton or alkali metal cations in the electrolyte and $MnO_\alpha(OC)_\beta$ and $MnO_{\alpha-\beta}(OC)_{\beta+\delta}$ represent manganese oxide in its high and low oxidation states, respectively. According to Eq. (9), the storage ability of the oxide is governed by the transport diffusion path length for both ions and electrons. As reported in the literature, the storage

ability of MnO_x is a function of both physical parameters (microstructure and morphology) and chemical ones (valence and hydrous state). Whereas high crystalinity of the oxide results in higher conductivity, the rigidity of the structure decreases the available surface area [3]. On the other hand, lower crystalinity tends to form highly porous structure but at the same time, the electrical conductivity of the sample will be low. This indicates that the real storage ability of the sample comes out of a trade-off between the electrical conductivity in the solid phase and the ionic transport in the pore [3]. Another very important factor is the valence of Mn in the oxide structure. The conductivity of the oxides containing Mn(III) is lower than their Mn(IV) counterparts due to Jahn-Teller tetragonal distortion.

Fig. 6 shows the calculated SC values for different scan rates ranging from 1 to 100 mV S^{-1}. As can be seen in the figure, the electrodeposition from the pure manganese nitrate solution (a) resulted in an SC value of 208 F g^{-1}. The addition of chrome at a Cr/Mn ratio of 2.5% (b) tend to cause a significant drop of the maximum SC to 52 F g^{-1} because of the presence of Mn(III) oxidation state. The lowest SC value was observed at a Cr/Mn ratio of 5% (c). The SC values increased by further increasing the Cr/Mn ratio, due to lower crystalinity and improved morphology of the sample, until reaching 281 F g^{-1} in the case of (e). In fact, where the Cr/Mn ratio is below 5%, the adverse effect caused by valence rendering is dominant whereas higher ratios tend to cause a positive effect due to morphological evolution and tuning of the crystallinity. The inset of Fig. 6 shows the cyclic voltammograms recorded at a scan rate of 1 V S^{-1}.

Fig. 7 shows galvanostatic charge/discharge profiles of electrode at current densitiey of 1A/g at 0–0.9 V vs. SCE. The results showed that the sample with high Cr/Mn ratio (10%) shows higher capacitance and this in agreement with cyclic voltammetry results.

Another important parameter for the electrochemical capacitor is life-cycle. As a high cycle life and long term stability warranty capacitors beneficial in many applications. The specific capacitance of the Cr doped electrode increases awhile during the first 250 cycles, which was owing to an activation process in the supercapacitor electrode, similar to the previous report [27] and then decreases gradually with a capacitance retention of 80% after 10,000 cycles of charging and discharging (Fig. 8).

4. Conclusion

In summary, Cr doped manganese oxide, which correlated the catalytic feature of Cr with the charge storage ability of the powdered manganese oxide, were successfully developed by a simple process. The product was characterized by XRD, DSC, FT-IR, SEM, and BET. The potential of the obtained sample for the supercapacitor application was evaluated. The SEM images clarified that the addition of Cr has a significant effect on the morphology and surface area of the samples and additional amounts of Cr tend to form flower-like nanostructures.

The electrochemical properties of the product were investigated by cyclic voltammetry. The electrochemical studies of the product elucidated that the doped metal oxide sample shows a good electrochemical behavior as a supercapacitor compared with the non-doped sample. The SC values increased by increasing the Cr/Mn ratio, due to lower crystalinity and improved morphology of the sample, until reaching 281Fg^{-1}. The sample exhibited gross cycling stability during 1000 cycles as it showed only 10% decay of capacity.

References

[1] Y. Zhang, H. Feng, X. Wu, L. Wang, A. Zhang, T. Xia, H. Dong, X. Li, L. Zhang, Int. J. Hydrog. Energ. 34 (2009) 4889–4899.
[2] M. Jayalakshmi, K. Balasubramanian, Int. J. Electrochem. Sci. 3 (2008) 1196–1217.
[3] G. Wang, L. Zhang, J. Zhang, Chem. Soc. Rev. 41 (2012) 797–828.
[4] A. Taguchi, S. Inoue, S. Akamaru, M. Hara, K. Watanabe, T. Abe, J. Alloy. Compd. 414 (2006) 137–141.
[5] D. Yan, Y. Li, Y. Liu, R. Zhuo, Z. Wu, B. Geng, J. Wang, P. Ren, P. Yan, Z. Geng, Mater. Lett. 117 (2014) 62–65.
[6] T. Yousefi, A.N. Golikand, M.H. Mashhadizadeh, M. Aghazadeh, Curr. Appl Phys. 12 (2012) 544–549.
[7] Z. Zeng, H. Zhou, X. Long, E. Guo, X. Wang, J. Alloy. Compd. 632 (2015) 376–385.
[8] J. Yu, L. Zhu, C. Fan, C. Zan, L. Hu, S. Yang, Q. Zhang, W. Zhu, L. Shi, F. Wei, Particuology 22 (2015), 2015, pp. 89–94.
[9] W. Li, J. Shao, Q. Liu, X. Liu, X. Zhou, J. Hu, Electrochim. Acta 157 (2015) 108–114.
[10] X. He, J. Wang, H. Jia, R. Kloepsch, H. Liu, K. Beltrop, J. Li, J. Power Sources 293 (2015) 306–311.
[11] H.R. Moazami, S.S.H. Davarani, T. Yousefi, H. Darjazi, Mat. Sci. Semicond. Proc. 38 (2015) 240–248.
[12] H.R. Moazami, S.S.H. Davarani, T. Yousefi, A.R. Keshtkar, Mat. Sci. Semicond. Proc. 30 (2015) 682–687.
[13] M. Pudukudy, Z. Yaakob, R. Rajendran, Mater. Lett. 136 (2014) 85–89.
[14] L.-X. Yang, Y.-J. Zhu, H. Tong, W.-W. Wang, Ultrason. Sonochem. 14 (2007) 259–265.
[15] M. Salavati-Niasari, F. Mohandes, F. Davar, K. Saberyan, Appl. Surf. Sci. 256 (2009) 1476–1480.
[16] O. Jankovský, D. Sedmidubský, P. Šimek, Z. Sofer, P. Ulbrich, V. Bartůněk, Ceram. Int. 41 (2015) 595–601.
[17] Q. Zhao, W.-H. Shih, Microporous Mesoporous Mater. 53 (2002) 81–86.
[18] M.W. Rophael, S.N. Boulis, Surf. Technol. 16 (1982) 243–248.
[19] T. Yousefi, M. Torab-Mostaedi, H.G. Mobtaker, A.R. Keshtkar, J. Nucl. Mater. 479 (2016) 633–638.
[20] S.C. Pang, M.A. Anderson, T.W. Chapman, J. Electrochem. Soc. 147 (2000) 444–450.
[21] T. Yousefi, A. NozadGolikand, M. Mashhadizadeh, M. Aghazadehc, J. Solid State Chem. 190 (2012) 202–207.
[22] S. Trasatti, Electrocatalysis of hydrogen evolution: progress in cathode activation, in: Advances in Electrochemical science and enginnering, Wiley-VCH, 2008.
[23] V. Yegnaraman, S. Vasudevan, Trans. SAEST 24 (1989) 223–227.
[24] T. Yoshida, D. Komatsu, N. Shimokawa, H. Minoura, Thin Solid Films 451 (2004) 166–169.
[25] V.M. Nikolic, S.L. Maslovara, G.S. Tasic, T.P. Brdaric, P.Z. Lausevic, B.B. Radak, M.P. Marceta Kaninski, Appl. Catal. B: Environ. 179 (2015) 88–94.
[26] J. Pattanayak, V.S. Rao, H.S. Maiti, Thermochim. Acta 160 (1990) 233–242.
[27] Y. Zhang, G. Li, Y. Lv, L. Wang, A. Zhang, Y. Song, B. Huang, Int. J. Hydrog. Energy 36 (2011) 11760–11766.